Investigation of the Effects of Filler Wires on the Microstructural and Mechanical Properties of GTAW-Welded IS2062E350C Pressure Vessel Steel

Alok Vardhan*, Abhishek Mishra** and Gajesh Kumar*

Keywords: GTAW, IS2062E350C, filler wires, tensile test, microhardness test, impact test, corrosion test, macrostructure and microstructure analysis.

ABSTRACT

Pressure vessels are vital across many industries for containing fluids under high pressures and temperatures. Their design, fabrication, and maintenance require strict standards for safety and reliability, with welding playing a crucial role. Extensive research has optimized welding practices, enhancing weld quality and mechanical properties. Studies have explored the impact of welding parameters and filler materials on performance. For example, research on materials like stainless steel and Inconel has revealed differences in mechanical strength, corrosion resistance, and weld quality based on filler wire selection. Gas Tungsten Arc Welding (GTAW) has been highlighted as a precise and versatile technique for creating high-quality welds in various industrial applications. Despite advancements, a research gap exists regarding the use of stainless-steel electrodes with low alloy mild steel, specifically IS2062E350C. This study aims to address this gap, comparing different filler wires to enhance cost efficiency and weld performance.

INTRODUCTION

Pressure vessels are critical components in many industries, primarily used to contain fluids under high pressure and temperature. These vessels are designed to withstand extreme operating conditions, which makes their design, fabrication, and maintenance highly demanding.

Paper Received June, 2024. Revised September, 2025. Accepted October, 2025. Author for Correspondence: Alok Vardhan.

Ensuring safety and reliability is paramount, and stringent standards govern the production of pressure vessels to prevent catastrophic failures. Welding plays a central role in the construction of these vessels, with various techniques and materials used to achieve strong, reliable joints that can withstand the intense pressures and temperatures typical in many industrial applications.

Over the years, extensive research has been conducted to improve welding practices and develop innovative techniques for welding pressure vessels. Welding technology has evolved significantly, with research focusing on understanding the effects of welding parameters, filler materials, and welding processes on the final weld quality. The selection of appropriate welding techniques and materials is critical to ensure that pressure vessels meet operational safety and performance standards.

Toudehdehghan et al. (2019) stressed the significance of understanding pressure vessel design principles, failure mechanisms, and regulatory standards. They highlighted welding's essential role in ensuring pressure vessel safety and performance. Welding parameters and filler materials are key factors that affect the structural integrity of these vessels. Bogdan et al. (2023) explored the effects of welding on P355N pressure vessel steel using molybdenum-alloyed copper demonstrating how welding techniques influence mechanical properties. Aravindkumar et al. (2021) examined 316L stainless steel joints and found that the nickel-coated filler materials they used altered the microstructure, particularly in the heat-affected zone Their SEM analysis showed high-temperature welding caused grain diffusion in the HAZ, leading to an increase in size. They also found that Ni-304 filler wire provided 1.8% higher hardness than plain 316L, with other fillers like Ni-316, Ni-308, and Ni-304 offering superior tensile strength and toughness.

Britto et al. (2020) focused on the effects of shielding gases in gas tungsten arc welding (GTAW) of T91 alloy steel tubes, revealing that helium shielding gas produced superior weld quality

^{*} Assistant Professor, Department of Mechanical Engineering, Ajay Kumar Garg Engineering College Ghaziabad, India.

^{**} Graduate Student, Department of Mechanical Engineering, Ajay Kumar Garg Engineering College Ghaziabad, India.

compared to other gases. Filler material selection was also shown to have a significant impact on the mechanical properties and corrosion resistance of welds. Kaur et al. (2014) examined the composition of filler wires in GTAW for stainless steel 202, comparing ER308L, ER316L, and ER310 fillers. ER308L provided the highest hardness and tensile strength, while ER316L and ER310 exhibited better corrosion resistance due to fewer inclusions. Naffakh-Moosavy et al. (2007) expanded on this by studying dissimilar welds between 310 austenitic stainless steel and Inconel 657, finding that Inconel fillers were less prone to hot cracking, making them suitable for extreme environments in industries like petrochemicals and nuclear energy.

Further studies explored the effects of different welding parameters and filler materials on specific materials used in pressure vessels. Mahajan et al. (2021) found that TIG welding with ER316L filler wire provided optimal tensile properties for SS304 joints in high-pressure applications. Jinkamon et al. (2023) analyzed dissimilar metal welding between carbon steel and 3CR12 stainless steel, determining that ER308L and ER309L filler wires offered satisfactory tensile strength and hardness for industries like sugar processing. Gurusamy et al. (2019) investigated the advantages of helium as a shielding gas in welding high-strength low-alloy (HSLA) steel, finding that its improved corrosion resistance and enhanced mechanical properties like tensile strength and hardness. Lastly, research by Prabakaran et al. (2015), Peasura et al. (2017), and Gaffar et al. (2017) showed how welding parameters and filler material choices can significantly influence weld strength and quality in various pressure vessel applications, while Kumar et al. (2017) demonstrated how parameter optimization using algorithms could improve the welding process further.

In summary, Gas Tungsten Arc Welding (GTAW) has established itself as a critical technique in pressure vessel fabrication due to its precision and versatility. It is particularly suited for welding thin to medium-thickness materials, where maintaining metallurgical integrity is essential. GTAW was selected for this study because of its ability to produce high-quality, defect-free welds with minimal heat-affected zones, ensuring optimal mechanical properties and corrosion resistance. The process also offers precise control over welding parameters, filler material composition, and shielding gases, making it highly reliable for demanding applications under extreme conditions.

Four filler wire variants: ER308L, ER309L, ER316L, and ER70S-2, were utilized in this research. These fillers were chosen for their varied chemical compositions and industrial relevance. Stainless-steel fillers (ER308L, ER309L, and ER316L) are recognized for their excellent corrosion resistance and mechanical strength, making them suitable for

stainless-steel welding. In contrast, ER70S-2, a low-alloy steel filler, is commonly used for mild steel applications and served as a baseline for comparison. Each filler wire was evaluated based on its unique characteristics and compatibility with specific welding requirements.

The selection of suitable filler materials plays a crucial role in optimizing weld quality, mechanical performance, and corrosion resistance. However, a knowledge gap exists regarding the application of stainless-steel filler wires in conjunction with low-alloy mild steel, particularly for pressure vessels. This research addresses this gap by investigating the influence of different filler wires on the microstructural and mechanical properties of IS2062E350C welds. The findings aim to refine welding practices and improve the fabrication of pressure vessels, contributing to advancements in the field of welding technology.

MATERIALS AND METHODOLOGY

Materials

Base material

The foundation of this research is based on the utilization of a 3 mm-thick sheet of IS2062E350C grade steel, as shown in Fig. 1(a). The decision to employ this material was guided by a thorough assessment of its mechanical properties, suitability for welding applications, and its relevance to the research objectives. Studies by Sadeghi et al. (2018) and Bogdan et al. (2023) investigated the effects of different process parameters on A537CL1 and P355N pressure vessel steels using the GTAW process. These materials possess properties similar to IS2062E350C, making the latter a viable choice for this study.



Fig. 1. Materials (a) Base Material (b) Filler Wires.

Typically, materials used for constructing pressure vessels are stainless steels, particularly for containers handling corrosive substances, high temperatures, and pressures. Additionally, a category of low-alloy pressure vessel steels is also utilized in industrial applications (Bogdan et al., 2023). IS2062E350C is a high-strength, low-alloy steel known for its durability and suitability for pressure vessel fabrication, with a minimum yield strength of 350 MPa. Thus, IS2062E350C is a promising material for general-purpose pressure vessel fabrication due to its

similarity in properties with other commonly used pressure vessel materials.

Table 1. Chemical composition of IS2062E350C Steel.

Element	Composition (%)		
С	0.158		
Si	0.0228		
Mn	1.04		
P	0.0158		
S	0.0037		
Cr	0.0213		
Ni	0.0174		
Al	0.05745		
Cu	0.0097		
W	0.0089		
Fe	98.6		

Upon receiving the material, a spectroscopy test was performed to determine the actual chemical composition of the base material. This test was carried out using a Spectrometer model SPECTROMAXX LMX10, manufactured by SPECTRO Analytical Instruments GmbH. The chemical composition of the IS2062E350C steel is presented in Table 1.

Filler Wire

This study utilized four filler wire variants: ER308L, ER309L, ER316L, and ER70S-2, all with a diameter of 1.6 mm, as shown in Fig. 1(b). These fillers were chosen for their diverse chemical compositions and widespread use in various industrial applications. ER308L, ER309L, and ER316L are stainless-steel fillers known for their exceptional corrosion resistance and mechanical strength, making them ideal for welding stainless steel. In contrast, ER70S-2, a low-alloy steel filler, is commonly used for mild steel applications and served as a benchmark for comparison in this study. Each filler wire offers unique properties designed to meet specific welding requirements and materials.

The specific properties of these filler wires make them suitable for a range of welding processes, ensuring optimal results in terms of strength, corrosion resistance, and weldability. ER309L filler wire, as highlighted by Madduru et al. (2014), is particularly employed for joining dissimilar metals, making it versatile in applications where different base metals need to be seamlessly welded together. Additionally, research by Kaur et al. (2014) underscores the suitability of ER316L filler wire for boiler applications, noting its robust mechanical properties and alloying elements that enhance performance in high-demand environments.

Both ER308L and ER316L have been noted for their ability to produce welds with higher tensile strength, as referenced by various studies. Vicente et

al. (2020) emphasized the excellent weldability of ER70S-2 filler wire, noting its ability to produce sound welds with minimal defects. The chemical composition of the filler wires is presented in Table 2

Table 2. Chemical composition of filler wire.

Filler Wire	ER308L	ER309L	ER316L	ER70S-2
C (%)	0.03	0.03	0.03	0.07
Cr (%)	19.5-22.0	23.0-25.0	18.0-20.0	0.15
Ni (%)	9.0-11.0	12.0-14.0	11.0-14.0	0.15
Mo (%)	0.75	9	2.0-3.0	0.15
Mn (%)	1.0-2.5	1.0-2.5	1.0-2.5	0.9-1.4
Si (%)	0.30-0.65	0.10-0.65	0.30-0.65	0.40-0.70
P (%)	0.03	0.02	0.03	0.025
S (%)	0.03	0.02	0.03	0.035
Cu (%)	0.75	0.75	0.75	0.5

Methodology Material Preparation

Rectangular sections with dimensions of 150 x 100 mm² and a thickness of 3 mm were cut from a raw sheet using a laser cutter, as shown in Fig. 2(a). The weld geometry and groove shape proposed by Elfallah (2023) are illustrated in Fig. 2(b). These sections feature a V-groove with a 60° angle, specifically designed to optimize welding results. The geometry and groove shape play a crucial role in ensuring the overall quality and integrity of the weld.

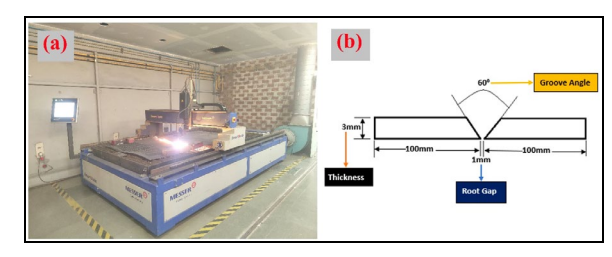


Fig. 2. Sample Preparation for Welding (a) Laser Cutter (b) V-groove Preparation.

Cleaning and Welding Preparation

Before welding, the sections were thoroughly cleaned using a grinding process to eliminate any contaminants that could interfere with the weld quality. The Gas Tungsten Arc Welding (GTAW) process was selected for this research due to its suitability for welding thin sheets (Aravindkumar, 2021). The welding was performed manually using a non-consumable tungsten electrode with a diameter of 2.4 mm, Argon shielding gas, and a DC current source with Direct Current Electrode Negative (DCEN) polarity. A root gap of 1 mm was maintained between the sheets, as illustrated in Fig. 2(b), to ensure proper joint formation.

Welding Procedure

The two sections were joined using the GTAW process with different filler wires (ER308L, ER309L, ER316L, and ER70S-2). The welding setup is depicted in Fig. 3. To reduce distortion in the weld, the process was conducted in two passes. The welding was carried out under controlled conditions, maintaining a constant current intensity of 100A throughout both passes. In the fixed current mode, the voltage varies to maintain a consistent arc current (Kutelu et al., 2018). Table 3 outline the welding parameters used for the first and second passes of the GTAW process.



Fig. 3. GTAW Welding Setup.

Table 3. Welding process parameter during welding.

Filler Wire	ER308L	ER309L	ER316L	ER70S-2
Current, (A)	100	100	100	100
Voltage, (V)	9.3	9.3	8.7	9.4
Travel Speed, (mm/min)	147.05	148.51	127.11	132.74
Heat Input, (KJ/mm)	0.227	0.225	0.246	0.255
Filler Diameter, (mm)	1.6	1.6	1.6	1.6



Fig. 4. Samples Preparation (a) Weldments (b) Wire-EDM.

To facilitate subsequent testing and analysis, samples were meticulously prepared from each weldment after the cooling phase, as shown in Fig. 4(a). The sample preparation involved the use of Wire-Electrical Discharge Machining (EDM), as depicted in Fig. 4(b), ensuring precision in preparing the samples for analysis.

Testing Procedure

The welded samples underwent various tests to their mechanical and metallurgical evaluate properties, including tensile testing, microhardness testing (Vickers test), corrosion testing, macrostructure and microstructure analysis, and impact testing. Each test required specific sample preparation methods, and the samples were prepared in accordance with the standards for the respective tests, as shown in Fig. 5. The samples were cut using a wire-EDM machine (Model: E Merge S64, Make: Electronica India Limited).

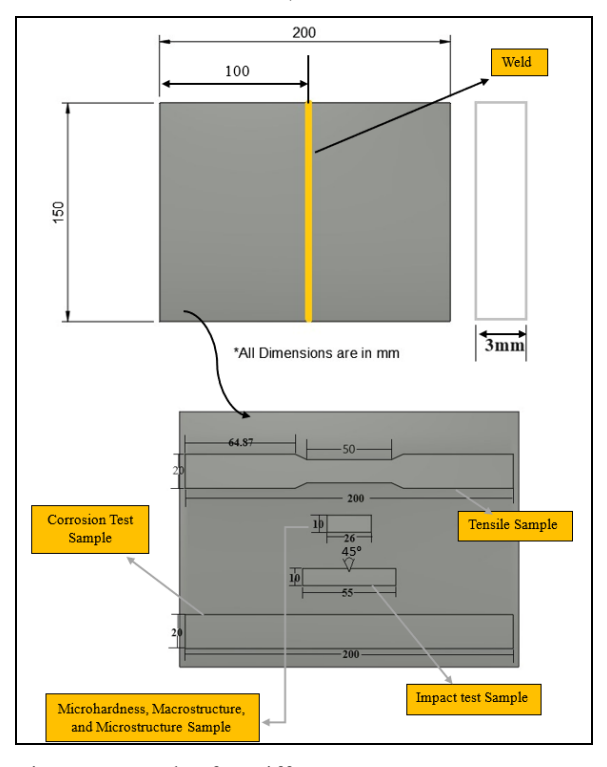


Fig. 5. Samples for Different Test.

Tensile tests were conducted on specimens prepared according to ASTM E8 standards. The samples were designed using CAD software and cut with precision through a CNC-operated wire-EDM machine. Testing was performed using a computerized Universal Testing Machine (UTM), Model UT 10 (Make: ENKAY), which has a range of 0-100kN. Both the base material and welded samples were sectioned into rectangular dimensions (26 x 10 mm²) for further microstructural and hardness testing. Prior to cutting, precise measurements were taken from the weld centre to ensure accuracy. For the microstructure, macrostructure, and microhardness analyses, the samples were mounted in epoxy using a Hot Mounting Press (Model: AUTOMOUNT, Make: METATECH Industries), then polished with silicon carbide emery paper and diamond paste. After polishing, the samples were etched with a nital reagent and prepared for analysis.

Macrostructure and microstructure analyses were performed using high-resolution microscopes. Macrostructure was examined with a digital

microscope (Model: Smart Zoom 5, Make: ZEISS), while microstructure was observed under a metallurgical microscope (Model: Stand Axio Observer 7, Make: ZEISS) at varying magnifications. Microhardness testing, in accordance with ASTM E-92 standards, was carried out using a Vickers hardness tester (Model: MV1-TS, Make: FIE) with a 0.3 kgf load applied for 9 seconds. The hardness was measured in different zones: Right Zone (RZ), Left Zone (LZ), and Weld Zone (WZ) and averages were calculated for each. Additional testing included the Charpy impact test, following ASTM E23 standards, using a pendulum-type machine (Model: IT 30 AUTO, Make: FIE) to evaluate fracture resistance. Corrosion testing was done with a Salt Spray Corrosion Test Chamber (Model: SST/HMI-480, Make: SRI Equipment), where samples were exposed to salt spray for 24 hours, followed by visual inspection and weight loss measurement to assess the corrosion extent.

RESULTS AND DISCUSSIONS

Tensile testing, microhardness testing (Vickers test), impact testing, corrosion testing, and macrostructure and microstructure analysis were conducted on the prepared samples. For each test, five samples were prepared: one from the base material and four from welded specimens. The results obtained from these tests are presented and discussed in the following sections.

Tensile Test

The tensile test was conducted on the prepared samples to evaluate their mechanical properties. This was performed using a computerized Universal Testing Machine (UTM). Each sample was subjected to axial loading until failure occurred, with load-displacement curves recorded throughout the test. The ultimate tensile strength (UTS) was then determined from the obtained data.

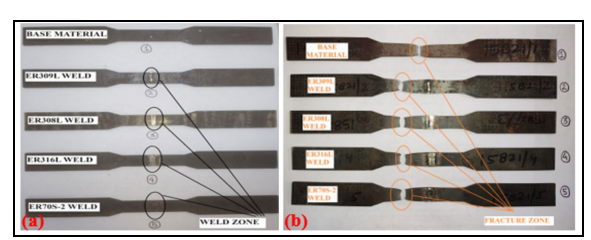


Fig. 6. Tensile Test Samples (a) Samples Before Tensile Test (b) Samples After Tensile Test.

The results revealed that all welded samples fractured in the parent material, IS2062E350C, indicating that the weakest region of the joints was the base material. Figure 6(a) shows the samples before the test, while Figure 6(b) displays the samples after the test. It is evident from the figures that the fractures occurred in the base material,

suggesting that the welds themselves were stronger than the base material.

Table 4. Ultimate Tensile Strengths (UTS) of Samples.

Sample No.	Material	UTS (MPa)
1	Base Material	550.14
2	ER309L Weld	584.55
3	ER308L Weld	567.41
4	ER316L Weld	560.12
5	ER70S-2 Weld	573.73

Table 4 summarizes the results, showing that the base material sample (1) exhibited an ultimate tensile strength of 550.14 MPa. This is lower compared to the tensile strengths of the welded samples, which were 584.55 MPa (sample 2), 567.41 MPa (sample 3), 560.12 MPa (sample 4), and 573.73 MPa (sample 5). Among the welded samples, the ER309L weld (sample 2) demonstrated the highest ultimate tensile strength of 584.55 MPa, indicating superior weld integrity and strength.

The results indicate that the use of filler wire in welding positively improves the strength of the joints. Grain size significantly affects mechanical properties and depends on the cooling rate. In this study, it is assumed that the cooling rate was consistent across all samples, so the differences in tensile strength are attributed to the alloying elements of the filler wires used.

Microhardness Test

Microhardness measurements were performed to evaluate the hardness distribution across the samples, as illustrated in Fig. 7(a). The Vickers hardness test was used, employing a Micro-Vickers Hardness Testing Machine depicted in Fig. 7(b). Indentations were made in three distinct regions: Right Zone (RZ), Weld Zone (WZ), and Left Zone (LZ). The average hardness values for each region are summarized in Table 5.

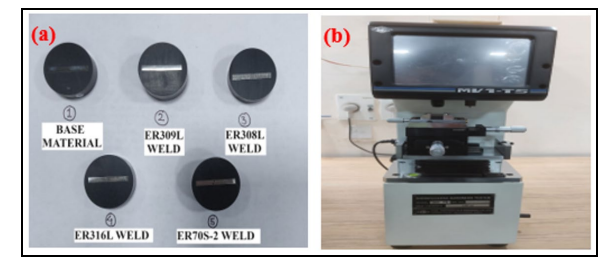


Fig. 7. (a) Samples for Micro-hardness Test (b) Vickers Hardness Testing Machine.

The base material exhibited a consistent average hardness of 179.33 HV. Among the welded samples, the Weld Zone (WZ) showed the highest hardness variations. The WZ of the ER308L welded sample demonstrated the maximum hardness at 459.28 HV, while the ER70S-2 welded sample recorded the

lowest at 277.97 HV, highlighting the significant impact of filler material choice on WZ hardness. Adjacent regions to the WZ experienced reduced hardness due to grain coarsening, a common effect of heat input during welding.

Table 5. Vickers Microhardness values of samples.

SAMPLE	ER309L	ER308L	ER316L	ER70S-2
	Weld	Weld	Weld	Weld
Right Zone	202.55	186.85	170.46	187 HV
(RZ)	HV	HV	HV	
Weld Zone	407.1	459.28	422.42	277.97
(WZ)	HV	HV	HV	HV
Left Zone	213.31	195.31	192.76	177.51
(LZ)	HV	HV	HV	HV

The hardness of the weldments and the Heat-Affected Zone (HAZ) is influenced by microstructural transformations. Fine-grained structures, which typically exhibit greater strength, tend to be replaced by coarser grains in the HAZ due to high heat input, resulting in lower hardness values. The ER70S-2 welded sample, subjected to higher heat inputs, exhibited lower average hardness in both the recrystallized and liquation zones compared to other samples.

Hardness in the WZ is predominantly determined by the filler material's chemical composition and the formation of carbide particles, which significantly increase hardness. Fine grain size also contributes to higher hardness levels. For example, the microstructure of the WZ in the ER308L welded sample, as shown in Fig. 23(b), reveals a fine-grained structure that accounts for its superior hardness. Although other samples exhibited similar grain sizes, the alloying elements in the filler wires had a more substantial influence on hardness.

Filler materials such as ER308L, ER309L, and ER316L, with higher concentrations of nickel (Ni) and chromium (Cr), enhance the mechanical properties of the welded joints. In the ER308L sample, these alloying elements, combined with a fine-grained microstructure and the formation of carbide particles, resulted in superior hardness and improved mechanical performance compared to the ER70S-2 filler wire.

Impact Test

The Charpy V-notch impact test was conducted to evaluate the impact toughness of the samples. Figures 8(a) and 8(b) show the samples before and after the impact test, respectively. The average absorbed energy for the base material and various weld metals is presented in Table-6. The results indicate that welded samples generally exhibited higher impact toughness compared to the base material (BM). Specifically, the sample welded with ER309L filler wire absorbed the highest impact toughness of 54.5 J, while the sample welded with ER70S-2 filler wire absorbed the lowest impact toughness of 35 J. The

ER308L welded sample showed the second-highest toughness at 51.5 J, followed by the ER316L welded sample with 39 J of toughness.



Fig. 8. Impact Test Samples (a) Impact Samples Before Test (b) Impact Samples After Test.

Table 6. Absorbed impact energy of samples.

Sample No.	Material	Absorbed Impact Energy (J)
1	Base Material	34
2	ER309L Weld	54.5
3	ER308L Weld	51.5
4	ER316L Weld	39
5	ER70S-2 Weld	35

The increased impact toughness in the welded samples compared to the base material highlights the significant role of filler wires in enhancing mechanical properties. This improvement is influenced by factors such as filler wire composition, heat input, and grain structure. Filler wires like ER308L, ER309L, and ER316L, enriched with alloying elements such as nickel (Ni) and chromium (Cr), significantly enhance the toughness of welded joints. In contrast, ER70S-2 lacks these elements, which explains its comparatively lower impact toughness.

Heat input is another critical factor affecting impact toughness. The ER70S-2 welded sample experienced higher heat input, as shown in Table 3, leading to grain growth. Larger grains can weaken fracture toughness by promoting crack initiation and (Gharibshahiyan propagation al., 2011). et Conversely. finer the grain structures stainless-steel filler-welded samples, such as those ER309L and ER308L, impede crack propagation and require more energy for crack initiation, as seen in Figures 22 and 23.

The impact toughness of the ER70S-2 welded sample (35 J) was nearly identical to that of the base material (34 J), likely due to their similar chemical compositions. On the other hand, the presence of austenite-stabilizing elements like Ni and Cr in ER308L, ER309L, and ER316L enhances their mechanical properties, resulting in superior impact toughness.

The exceptional toughness of 54.5 J observed in ER309L-welded samples can be attributed to its enriched alloy composition, particularly its high Ni and Cr content. These elements not only improve

durability but also contribute to a fine-grained microstructure that effectively resists crack propagation. Additionally, optimized welding parameters further enhance the toughness of ER309L, making it superior to other filler wires in terms of impact resistance.

Corrosion Test

The corrosion test was conducted to assess the samples' resistance to corrosive environments, a critical factor in oil and gas industries. The results revealed that all samples, including both the base material and the four welded samples, performed well in the test. Figures 9(a) and 9(b) show the samples before and after the test. Visual inspection of the Welded Zone (WZ) indicated that the welds with ER309L (2), ER308L (3), and ER316L (4) exhibited minimal corrosion, while the weld with ER70S-2 (5) showed significantly higher corrosion.

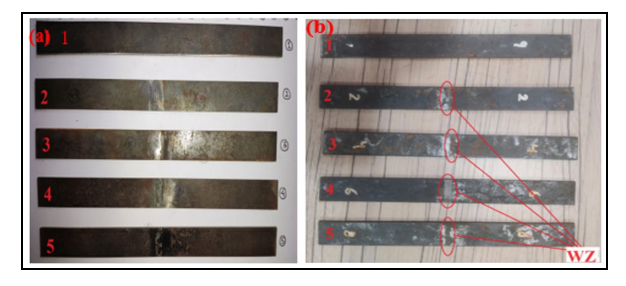


Fig. 9. Corrosion Test Samples (a) Samples Before Corrosion Test (b) Samples After Corrosion Test.

Table 7. Weight Measurements of Samples in Corrosion Test.

SAMPLE	Weight before test (gm)	Weight after test (gm)	% Reduction in weight
Base Material (1)	93 gm	86 gm	7.52%
ER309L Weld (2)	88 gm	81 gm	7.95%
ER308L Weld (3)	91 gm	84 gm	7.69%
ER316L Weld (4)	91 gm	87 gm	4.39%
ER70S-2 Weld (5)	92 gm	82 gm	10.86%

The observed results are closely linked to the alloy composition of the filler materials. Stainless-steel fillers such as ER308L, ER309L, and ER316L are enriched with nickel (Ni) and chromium (Cr), which significantly enhance their corrosion resistance. In contrast, ER70S-2 lacks these critical elements, resulting in inferior performance against corrosion. According to Kaur et al. (2014), the weld metal contains two distinct particle types: white particles, which have lower Cr and Ni but higher levels of carbon (C), oxygen (O), silicon (Si), and aluminum (Al), and black particles, which are rich in Cr and Ni, contributing to better corrosion resistance. As

illustrated in Figures 12-14, weld metals using ER308L, ER309L, and ER316L show a greater presence of black particles, indicating higher Cr and Ni levels. In comparison, Figure 15 highlights a predominance of white particles in the ER70S-2 weld metal, correlating with its lower corrosion resistance.

Table 3 further supports these findings, confirming the higher concentrations of Ni and Cr in ER308L, ER309L, and ER316L, which account for their superior performance in corrosive environments.

Among these, the ER316L welded sample demonstrated the best corrosion resistance, with the lowest weight reduction percentage (4.39%). This is primarily due to its high Ni and Cr content, which forms a protective passive oxide layer that shields the material from corrosive attacks. The addition of molybdenum (Mo) further improves its resistance to pitting and enhances its durability in chloride-rich environments, such as those in the oil and gas industry. This combination of alloying elements makes ER316L exceptionally resistant to corrosion compared to other filler materials.

Macrostructure Analysis

A macrostructure analysis was performed to assess the presence of different phases, defects, and the homogeneity of the welded material. Figures 10(a) through 10(d) display the macrostructure images of all welded samples. The images of samples welded with ER309L and ER308L filler exhibit higher weld uniformity and integrity compared to those welded with ER316L and ER70S-2 filler wires.

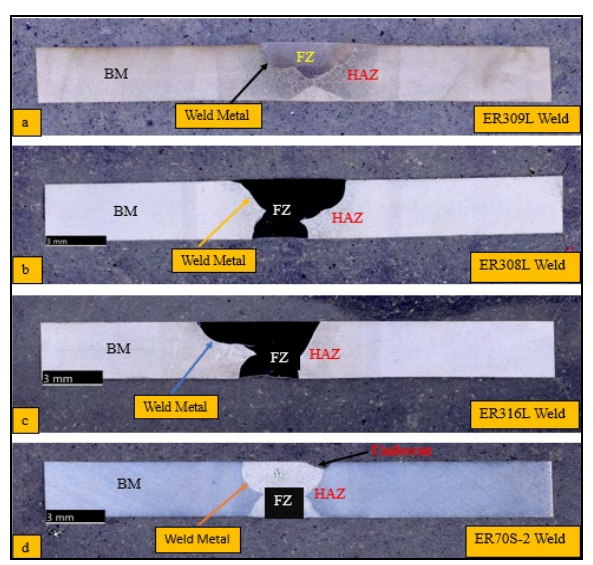


Fig. 10. Macrostructure Images of Welded Samples (a) ER309L Welded Sample (b) ER308L Welded Sample (c) ER316L Welded Sample (d) ER70S-2 Welded Sample.

In the macrostructure images, the Heat Affected Zone (HAZ) is clearly visible, and the properties near the HAZ show slight deviations from the Base Metal (BM). A notable defect, known as undercut, was

observed in the ER70S-2 welded sample. This defect likely resulted from high heat input that melted part of the base material without adequately filling it. The shape of the fusion zone is primarily influenced by heat input, which is dependent on current, voltage, and travel speed.

In this study, the welding current was fixed at 100A, while the voltage was varied to maintain a constant arc current. Therefore, voltage and travel speed could have been significant factors affecting structural changes. Figure 10(a) shows the macrostructure of the ER309L weld, which has a smaller face and root width compared to the other samples. Figures 10(b) and 10(c) illustrate the macrostructures of ER308L and ER316L welded samples, respectively, both of which have significantly larger face widths. Figure 10(d) depicts the macrostructure of the ER70S-2 welded sample, where a well-formed weld bead structure is observed due to the effective mixing of the filler wire with the base material, despite high heat input.

High heat input melts both the base metal and filler wire, facilitating proper mixing. As the mixability increases, the molten metal's weight causes it to move downward to the root of the welded joint, forming a more uniform shape (Jinkamon, 2023). Although the ER309L welded sample had the highest travel speed, indicating minimal HAZ width, the macrostructure images reveal a larger HAZ width, suggesting a lower influence of travel speed.

All samples exhibited complete penetration with no defects, except for the ER70S-2 sample. The HAZ experienced significant heat input, leading to microstructural changes and grain coarsening, which affected the material's properties. The ER316L welded sample displayed less uniform root penetration, with discontinuities observed in the root section.

Microstructure Analysis

The microstructure analysis of the base material (IS2062E350C) and various welded samples has provided valuable insights into the effects of different filler wires and welding parameters. The distinct zones: Base Metal (BM), Fusion Zone (FZ), and Heat Affected Zone (HAZ), display variations in their microstructural properties, which are crucial for understanding the mechanical performance of the welded joints.

Figure 11 shows that the base material, IS2062E350C steel, primarily consists of ferrite and pearlite. The fine-grained structure observed in Figure 11(b) suggests a balanced combination of strength and ductility. Figure 12 illustrates the microstructure of the welded sample using ER309L filler wire. In this case, the FZ exhibits a mix of austenitic and ferritic phases, characteristic of ER309L, an austenitic stainless-steel filler. The presence of the HAZ near the weld interface is

evident, with noticeable grain coarsening (Fig. 12a, 12c). This grain growth in the HAZ can increase brittleness, affecting the weld's mechanical integrity.

The microstructure of the ER308L welded sample, shown in Figure 13(a), reveals distinct regions of BM, HAZ, and FZ. The disparity in grain size and structure between these zones is evident from Figures 13(b), 13(c), and 13(d). Coarser grains in the HAZ (Fig. 13a, 13c, 13d) result from the thermal cycle during welding. ER308L, another austenitic stainless-steel filler, contributes to a dendritic structure in the FZ, enhancing mechanical strength and toughness, as supported by hardness and toughness results.

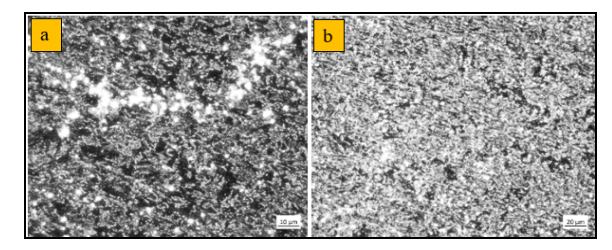


Fig. 11. Microstructure of Base Material (a) at $10\mu m$ and (b) at $20\mu m$.

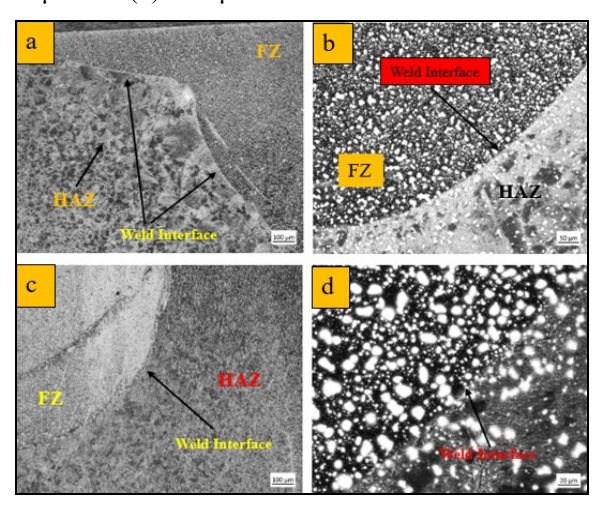


Fig. 12. Microstructure of ER309L Weld (a) showing HAZ, FZ, weld interface of left portion at $100\mu m$ (b) HAZ and FZ at $50\mu m$ (c) HAZ, FZ of right portion at $100\mu m$ (d) FZ and weld interface at $20\mu m$.

Figure 14(b) presents the microstructure of the ER316L weld, showcasing a tree branch-like dendritic structure in the FZ. This structure, typical of stainless-steel welds, forms during the solidification of molten metal and provides improved mechanical properties. The distinct boundary between the FZ and BM highlights the metallurgical changes due to welding.

The ER70S-2 filler wire weld, depicted in Figure 15, shows a clear distinction between the FZ and BM.

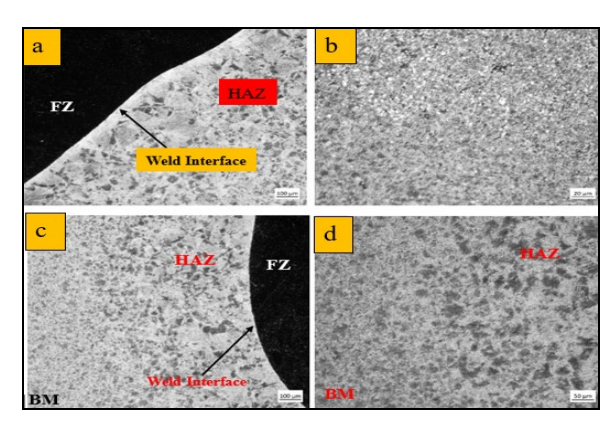


Fig. 13. Microstructure of ER308L Weld (a) weld interface, FZ, HAZ at $100\mu m$ (b)FZ and HAZ at $20\mu m$ (c) BM, FZ and HAZ at $100\mu m$ (d) BM and HAZ at $50\mu m$.

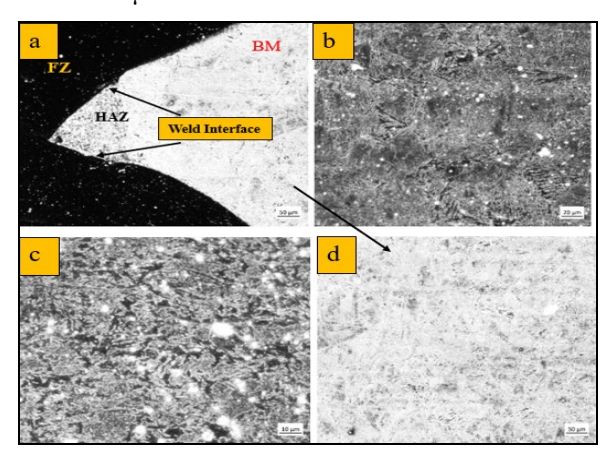


Fig. 14. Microstructure of ER316L Weld (a) disparity in FZ, BM and HAZ at 50μm (b) microstructure at 20μm (c) microstructure of FZ at 10μm and (d) microstructure of BM at 50μm.

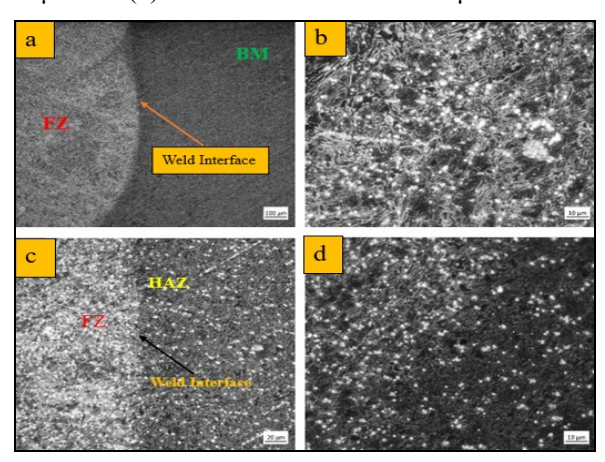


Fig. 15. Microstructure of ER70S-2 Weld (a) showing disparity between BM and FZ at $100\mu m$ (b) FZ microstructure at $10\mu m$ (c) difference in HAZ and FZ at $20\mu m$ and (d) FZ and HAZ at $10\mu m$.

Figure 15(a) indicates differences at the weld interface, with Figure 15(c) showing a higher content of white particles in the FZ, signifying increased ferrite content. This is consistent with the higher iron

content in ER70S-2. Figures 15(b) and 15(d) detail the microstructural constituents, emphasizing the varying grain sizes between the FZ and BM.

In all welded samples, finer grains are observed in the BM, while the HAZ exhibits coarser grains. The extent of the HAZ and its grain structure varies with different welding parameters, such as voltage and travel speed. This study confirms that varying heat inputs result in differences in the HAZ area and FZ shape, which contrasts with Bansod (2023), who reported a consistent HAZ area with uniform heat input. The coarser grains in the HAZ, due to thermal exposure during welding, negatively impact mechanical properties like toughness and hardness. The dendritic structure in the FZ of the ER316L welded sample enhances mechanical strength and toughness, crucial for high-performance applications.

CONCLUSIONS AND FUTURE SCOPE OF WORK

This study has comprehensively analyzed the impact of various filler materials and welding parameters on the mechanical and microstructural properties of welded joints. Through tensile, microhardness, Charpy impact, corrosion tests, and macrostructural and microstructural analyses, the research that filler demonstrates materials significantly influence weld performance. ER309L exhibited superior tensile strength and impact toughness compared to other fillers, highlighting the critical role of alloying elements in enhancing weld quality. The findings also indicate that ER70S-2, while having comparable impact toughness to the base material, showed lower hardness and corrosion resistance, making it less suitable for environments with high corrosion risk.

The novelty of this research lies in its holistic approach, integrating mechanical testing with detailed microstructural and macrostructural analysis to provide a comprehensive understanding of how different fillers and welding conditions affect joint performance. The study presents significant insights into the microstructural transformations in the Heat-Affected Zone (HAZ) and Fusion Zone (FZ), demonstrating the influence of alloying elements like Ni and Cr on weld integrity. This research offers a valuable framework for selecting optimal welding materials and parameters, particularly for critical applications like pressure vessels, where strength, toughness, and corrosion resistance are essential.

In terms of impact, this study has direct implications for pressure vessel welding, where the quality of welds under high pressure and corrosive environments is critical. By demonstrating that fillers like ER309L and ER316L offer superior mechanical properties and corrosion resistance, the research provides key guidance for improving the safety and durability of pressure vessels. Future work could

focus on exploring the long-term behavior of these welds in extreme pressure and temperature conditions, further refining welding techniques to ensure maximum reliability in industries such as oil and gas, chemical processing, and power generation.

REFERENCES

- Aravindkumar, D. and Thirumalai R., "Investigations on Microstructural Characteristics and Mechanical Properties of 316 L Stainless Steel Welded Joints Using Nickel Coated Filler Material by Gas Tungsten Arc Welding," *Material Research Express* 8 (4): 046513 (2021).
- Bansod, A, "Influence of Filler Wire on Metallurgical, Mechanical, and Corrosion Behaviour of 430 Ferritic Stainless Steel Using a Fusion Welding Process," *Material Research Express* 10 (3), (2023).
- Bogdan, C., and Vasile G.C, "X-ray Analysis of Welding Parameters Influence on Pressure Vessel Steel P355 N," *Journal of Physics:* Conference Series 2540: 012040 (2023).
- Britto, J., John R.A., Prabhakaran, G.M.R., Jeya J.J., and Mageshwaran G, "Enhancement of Mechanical Properties of Alloy Steel by GTAW with Different Purge/Shielding Gases," *FME Transactions* 48: 149-154 (2020).
- Elfallah, S, "Influence of Groove Shape on the Mechanical Properties of Welded Commercial Steel," Welding Technology Review 95: 49–56 (2023).
- Gaffar, Md., "Experimental Investigation on Welded Joints of Dissimilar Steels," *International Journal of Current Engineering and Technology* 7 (3), (2017).
- Gharibshahiyan, E., Abbas H.R., Nader P., and Mehdi R, "The Effect of Microstructure on Hardness and Toughness of Low Carbon Welded Steel Using Inert Gas Welding," *Materials & Design* 32 (4): 2042-2048 (2011).
- Gurusamy, D., Soundararajan R., Prashanth M., Senthilkumar R., and Sivakumar N, "Mechanical and Metallurgical Analysis of HSLA Steel for Gas Tungsten Arc Welding with Different Shielding Gases," *SAE Technical Paper* 2019-28-0069 (2019).
- Jinkamon, L, "Investigation of ER308L and ER309L Filler Wires on Dissimilar Metals between Carbon Steel and 3CR12 Ferritic Stainless Steel by GTAW through Boiler Fabrication in a Sugar Factory," *Material Research Express* 10: 126501 (2023).
- Kaur, G., Singh D., and Grewal J, "Effect of Filler Wire Composition on Joining Properties of GTAW Stainless Steel 202," In *Proceedings*

- of the International Conference on Research and Innovations in Mechanical Engineering, 191–200 (2014).
- Kumar, R., Mevada, N., Rathore, S., Agrawal, N., Rajput, V., and Barad A.P, "Experimental Investigation and Optimization of TIG Welding Parameters on Aluminum 6061 Alloy Using Firefly Algorithm," *IOP Conference Series: Materials Science and Engineering* 225: 012153 (2017).
- Kutelu, B.J., Saliu O.S., Godwin I.E., and Ayotunde I.I, "Review of GTAW Welding Parameters," *Journal of Minerals and Materials Characterization and Engineering* 6 (5): 541–554 (2018).
- Madduru, P.R., William, A., Prashanth, M., Kumar, S.N., Ramkumar, K.D., Arivazhagan, N., and Narayanan, S, "Assessment of Mechanical Properties of AISI 4140 and AISI 316 Dissimilar Weldments," *Procedia Engineering* 75: 29–33 (2014).
- Mahajan, A., Singh, H., Kumar, S., and Kumar S, "Mechanical Properties Assessment of TIG Welded SS 304 Joints," *Materials Today: Proceedings* 56 (2021).
- Naffakh-Moosavy, H, "A Comparative Evaluation of Welding Consumables for Dissimilar Welds between 310 Austenitic Stainless Steel and Inconel 657," *International Journal of ISSI* 4 (1-2): 39-49 (2007).
- Peasura, P, "Investigation of the Effects of Submerged Arc Welding Process Parameters on the Mechanical Properties of Pressure Vessel Steel ASTM A283 Grade A," *Journal* of Engineering, Article ID 9048324 (2017).
- Prabakaran, M.P, "Investigation of Mechanical Properties and Microstructure of GTAW on Dissimilar Metals," *International Journal of Applied Research* 1: 97–99 (2015).
- Sadeghi, B., Hassan S., Mahdi R., and Morteza, T, "Effects of Post Weld Heat Treatment on Residual Stress and Mechanical Properties of GTAW: The Case of Joining A537CL1 Pressure Vessel Steel and A321 Austenitic Stainless Steel," *Engineering Failure Analysis* 94: 396–406 (2018).
- Toudehdehghan, A., and Tan H, "A Critical Review and Analysis of Pressure Vessel Structures," *IOP Conference Series: Materials Science and Engineering* 469: 012009 (2019).
- Vicente, A, "The Correct Choice among Welding Wires ER70S-2, ER70S-3 and ER70S-6, According to the Oxidation Level of Base Metal," *International Journal of Advanced Engineering Research and Science* 7 (8): 131–139 (2020).